IEEE Access
Multidisciplinary ⋮ Rapid Review ⋮ Open Access Journal

Received 4 May 2023, accepted 2 June 2023, date of publication 8 June 2023, date of current version 15 June 2023.

Digital Object Identifier 10.1109/ACCESS.2023.3283983

RESEARCH ARTICLE

Design and Implementation of an Improved Finite-State Predictive Direct Torque Control for Induction Motor With New Weighting Factor Elimination

MOHAMED CHEBAANI[1], MOHAMED EBEED[2,3], WALID S. E. ABDELLATIF[4], Z. M. SALEM ELBARBARY[5], AND NOURA A. NOURALDIN[4]

[1]Department of Electrical Engineering, LGEB Laboratory, University of Biskra, Biskra 07020, Algeria
[2]Department of Electrical Engineering, EPS Linares, University of Jaén, 23700 Jaén, Spain
[3]Department of Electrical Engineering, Faculty of Engineering, Sohag University, Sohag 82524, Egypt
[4]Electrical Department, Faculty of Technology and Education, Suez University, Suez 43533, Egypt
[5]Department of Electrical Engineering, College of Engineering, King Khalid University, Abha 61421, Saudi Arabia

Corresponding author: Noura A. Nouraldin (Noura.Nouraldin@ind.suezuni.edu.eg)

This work was supported by the Deanship of Scientific Research at King Khalid University through the General Research Project under Grant RGP.1/373/44.

ABSTRACT The performance enhancement of the Induction Motor (IM) is a crucial and strenuous task. The Direct Torque Control (DTC) method is a common control strategy for boosting the IM drives and wildly implemented due to its merits including insensibility to motor parameters and fast response. However, the main shortage of the traditional DTC method is that it may lead to large flux and torque ripples. In this regard, this paper proposes an efficient control method called a Finite-State Predictive Torque Control (FS-PTC) which is based on multi objective optimization technique to overcome the shortage in the conventional DTC method. In addition to that a ranking approach is presented to assign the weighting factor in the cost function which directly affects the performance of system. The proposed ranking approach is based on elimination the weighting factor by replacing the single cost function with two different cost functions. The proposed FS-PTC is applied and tested using the dSPACE environment to validate its effectiveness and efficacy. From the experimental simulations, the performance of system is enhanced considerably where the torque and flux ripples are reduced with maintaining a constant switching frequency compared to the conventional DTC.

INDEX TERMS DTC, FS-PTC, flux ripples, torque ripples, constant switching frequency, dSPACE.

NOMENCLATURE

i_r, i_s	The rotor and stator currents
$\vec{\psi}_r, \vec{\psi}_s$	The rotor and stator flux vectors.
$\vec{\psi}_s^*$	Reference stator flux.
$\vec{v}_\circ$	Stator voltage vector
T_e	Electromagnetic torque.
T_l	Load torque.
L_s, L_r	The stator and the rotor windings leakage inductance.
$\tau_r = \frac{L_r}{R_r}$	The rotor time constant.
ω_m	The rotor speeds.
ω_e	The rotor frequency.
V_{dc}	Voltage of Dc-link.
J	The inertia moment.
p	The pole pairs number.
$v_\circ \ldots . v_7$	Possible voltage vectors.
$T_e^*(k+1)$	Predicted reference torque.
$k_r = \frac{L_m}{L_r}$	Rotor coupling factor.
R_s, R_r	Stator and rotor resistances.
$\vec{\psi}_s^p$	Predicted stator flux.
I	Vector sum.
R_σ	Equivalent resistance referred to stator.

The associate editor coordinating the review of this manuscript and approving it for publication was Xiwang Dong.

L_σ	Leakage inductance of stator.
L_m	Mutual inductance.
σ	Total leakage parameter.
τ_σ	Transient time stator constant.
T_e^*	Reference electromagnetic torque.
λ_p	Stator flux weighting factor.
λ_n	Switching frequency weighting factor.
T_s	Sampling time.
$S_x\ (k+1)$	Switching state for the next time instant $k+1$.
$T_e^p(k+1)$	Predicted torque.

I. INTRODUCTION

In many electrical drive industry applications, quick and precise torque control with decrease current harmonic distortion is a mandatory condition [1]. Fundamentally, there are two control techniques for AC motor drives: DTC and Field Orientation Control (FOC) [2], [3]. FOC technique presents good flux control and dynamic torque with the constant switching frequency and has taken great interest in the industries [4]. However, it has a complex control structure by the use of two (PI) controllers, axis transformation, and Space Vector Modulation (SVM) blocks. Furthermore, the powerfulness of the controller has a large parameter dependency. On the other hand, DTC has a simple structure, without axis transformation or modulation blocks, and has made an appearance in place of the FOC strategy method [5], [6]. The perfectly suitable the inverter's voltage vector is chosen using the DTC method using a predetermined switching table relied on error signs and stator flux position of flux and torque. The controller confers an extremely rapid dynamic response. However, DTC has two weaknesses: the torque ripples are significant, especially when compared to the FOC, and the switching frequency is unpredictable and based on the hysteresis bands [7]. Resulting of advancements in numerical calculation and real-time implementation tools [8], the model predictive control (MPC) has featured as a highly beneficial and alluring control method in a variety of industry applications [9], [10]. This control method is based this is using the controller dynamic model to predict in real-time the process's future attitude and the cost function is assess the control's goals and effectiveness. The cost function can comprise several variables and restrictions with suitable weighting factors and allow for simultaneous control. The picked optimum control measures are implemented in the controlled system. It is relatively novel to use MPC in electrical machines and power converters. Electrical machines have been subjected to a variety of MPC control approaches, including generalized model predictive control (GPC) [11], [12], finite control set-model predictive control (FS-MPC) [13], [14] and dead-beat predictive control [15]. Numerous predictive-based strategies were investigated in order to guarantee lower torque ripples and steady switching frequency running. Predictive torque control (PTC) also displays the benefit of not having an internal current control loop [16]. Compared to the well-traditional FOC approach, the finite control set-predictive torque control (FS-PTC) enables rapid dynamic reactions [17]. The FS-PTC structure is less complex than the traditional DTC. In FS-PTC, stator flux and torque are foretelling for a limited number of possible switching cases of the Voltage Source Inverter (VSI). The switching case that reduces flux ripples and torque is selected as the best one depended on the predefined cost function. [18]. In [16], a popularized two-vector-based MPC is suggested to guarantee low torque error using FS-PTC. The listing of whole possible voltage vectors is avoided using a deadbeat solution to lessen the computational load [15], [19]. In [20] and [21], depending on the placement of the sign of error in the stator flux and stator flux, the number of potential forecast vectors is decreased. Although there are still more calculations, a different decreased switching selection technique is proposed that uses an extended prediction horizon to lessen torque ripples in [23] and [24]. There are various methods, such as a single prediction method, to decrease the number of computations and hence streamline the MPC design [25].

The system performance relies on the choice of a weighting factor in the cost function. The critical issue with FS-PTC implementations is the choice of a suitable weighting factor. Weighting factors are utilized to stabilize the various control objectives and offer one or another variable more importance. The selection of these factors is a difficult task. A few techniques for choosing the optimum weighting factors for the system's performance have been presented in the literature. In [27], the various-objective optimization-based ranking approach in the cost-function of PTC eliminated the chosen of weighting factors. The computational difficulty rises rapidly with the excess in the number of switching cases or foretelling horizons. Optimum choice of the weighting factor for PTC was demonstrated in [28]. These techniques provided less torque ripple compared with traditional PTC. Nevertheless, the choosing of an optimized weighting factor is complex and dependent on induction motor parameters.

This paper presents method to diminish the weighting factors requirement of the FS-PTC technique. The major idea is the independent assigning of two various cost functions for the converter voltage vectors, followed by the calculation of the ranking of each potential solution utilizing a novel technique without the need for computationally intensive calculations. This study has investigated extensively the performance in terms of average switching frequency, torque ripples, and flux ripples. At the particular operation point, the dynamic performance of the proposed FS-PTC has been contrasted with that of another techniques, such as DTC and FS-PTC with average switching frequency reduction. Furthermore, A distinguishing feature of the proposed FS-PTC is the reduction of the average switching frequency and the demonstration of its variation in a relatively narrow frequency range. A dSPACE DS1104 controller board with Control Desk and MATLAB/Simulink software are used

to implement the proposed control technique. Extensive experimentation is used to confirm the proposed controller's effectiveness.

The following is a summary of the article's contributions:

1) Studying and developing the strategies based on FS-PTC to control induction motors by multi-objective optimization techniques as opposed to a single-cost function depended on weighting factors.

2) Comparing the dynamic performance of the proposed FS-PTC with other techniques such as FS- PTC and DTC with average switching frequency decrease at particular operation points.

3) The DS1104 control board is utilized to carry out the experimental validation and compared with the simulation results.

This paper has been organized as follows: Section II explains the model of the power system based on IM. Section III gives an overview of the classical DTC and FS-PTC. Section IV shows the experimental setup, which comprised of the dSPACE 1104 controller board, and also the hardware simulation results. Finally, conclusions are presented in Section V.

II. SYSTEM MODELING

A. MODEL OF INDUCTION MOTOR

The IM model can be described as follows:

$$\overrightarrow{v_s} = R_s \overrightarrow{i_s} + \frac{d\overrightarrow{\psi_s}}{dt} \tag{1}$$

$$0 = R_r \overrightarrow{i_r} + \frac{d\overrightarrow{\psi_r}}{dt} - j\omega_e \overrightarrow{\psi_r} \tag{2}$$

$$\overrightarrow{\psi_s} = L_s \overrightarrow{i_s} + L_m \overrightarrow{i_r} \tag{3}$$

$$\overrightarrow{\psi_r} = L_m \overrightarrow{i_s} + L_r \overrightarrow{i_r} \tag{4}$$

$$T_e = 1.5\, p\, I\, m\, \overrightarrow{\psi_s^*} \cdot \overrightarrow{i_s} \tag{5}$$

$$J\frac{d\omega_m}{dt} = T_e - T_l - f\omega_m \tag{6}$$

B. TWO-LEVEL VOLTAGE INVERTER MODEL

In this article, both the traditional DTC and the PTC technique employ a two-level VSI. The configuration of the VSI and its possible voltage vectors are demonstrated in Fig.1. Taking into account that each inverter phase's two switches function in a complimentary mode to prevent short-circuiting. This topology has eight possible switching states (finite states), which produce seven different voltage vectors. Six of them (v_1 to v_6) are active vectors and the other two (v_0 and v_7) are called zero vectors. The voltage and current variables of the three-phase system can be represented by a three-axis coordinate system.

The following vector can be used to represent the switching state (S):

$$S = \frac{2}{3}S_a + aS_b + a^2S_c \tag{7}$$

TABLE 1. Voltage vectors for two level-VSI.

v_n	$v = v_\alpha + jv_\beta$	$S = S_a, S_b, S_c$
v_0	0	[0,0,0]
v_1	$\frac{2}{3}V_{dc}$	[1,0,0]
v_2	$\frac{1}{3}V_{dc} + j\frac{\sqrt{3}}{3}V_{dc}$	[1,1,0]
v_3	$-\frac{1}{3}V_{dc} + j\frac{\sqrt{3}}{3}V_{dc}$	[0,1,0]
v_4	$-\frac{1}{3}V_{dc}$	[0,1,1]
v_5	$-\frac{1}{3}V_{dc} - j\frac{\sqrt{3}}{3}V_{dc}$	[0,0,1]
v_6	$\frac{1}{3}V_{dc} - j\frac{\sqrt{3}}{3}V_{dc}$	[1,0,1]
v_7	0	[1,1,1]

where $a = e^{j2\pi/3}$, $S_i = 1$ indicates S_i ON, $S_i = 0$ indicates OFF, and $i = a, b, c$. The voltage vector v is linked to the switching state S according to the following equation:

$$v = V_{dc}S \tag{8}$$

Considering all potential combinations of the gating signal S_a, S_b and S_c, eight voltage vectors, and eight switching states are illustrated in Table 1.

III. DIRECT TORQUE CONTROL

All DTC-based control systems primarily rely on the precise appreciation of stator flux, which is accomplished by utilizing currents and voltage of the stator. As defined by [1] and [2] respectively, there are two various groups of stator flux appreciators that rely on the voltage and current model. The appreciator utilizing the voltage model needs lower parameters than the one that relies on the current model. The DC drift of current sensors prevents the ideal integrator in [1] from functioning correctly in a practical implementation. DC drifts in stator current measurements are unavoidable due to the design of the signal conditioning circuits and current sensors. During the integration process, DC drift errors build up and cause instability in the machine drive system. Instead of the ideal integrator, the low pass filter (LPF) is the approach that is most frequently used. The LPF is always capable of carrying out the integration task under normal operational conditions. When the signal is DC, the gain for LPF compensation becomes infinite and the filter time constant, making it impossible to conduct the integration. But the LPF would create errors of the magnitude and phase angle, and the controller becomes more complicated due to the additional procedures to correct the defects. Figure 2 demonstrates the whole DTC scheme.

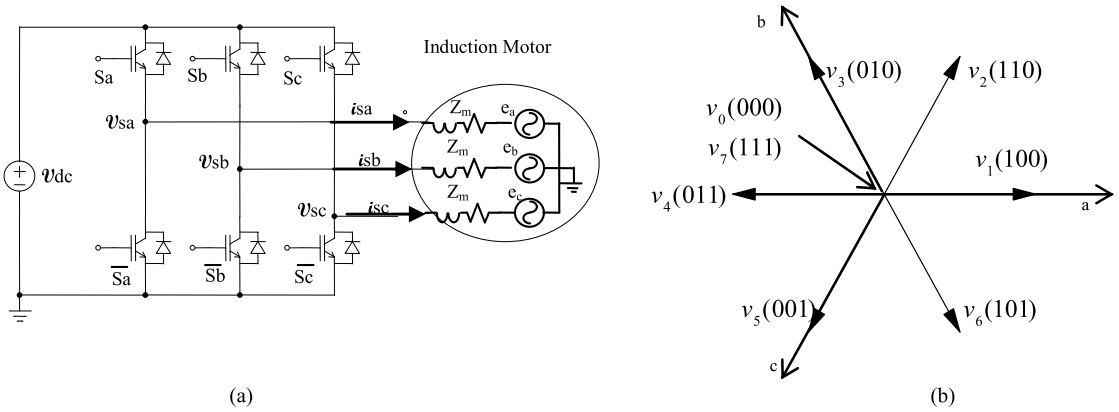

FIGURE 1. Two level voltage source inverter (2L-VSI). (a) Power circuit; (b) Voltage vectors.

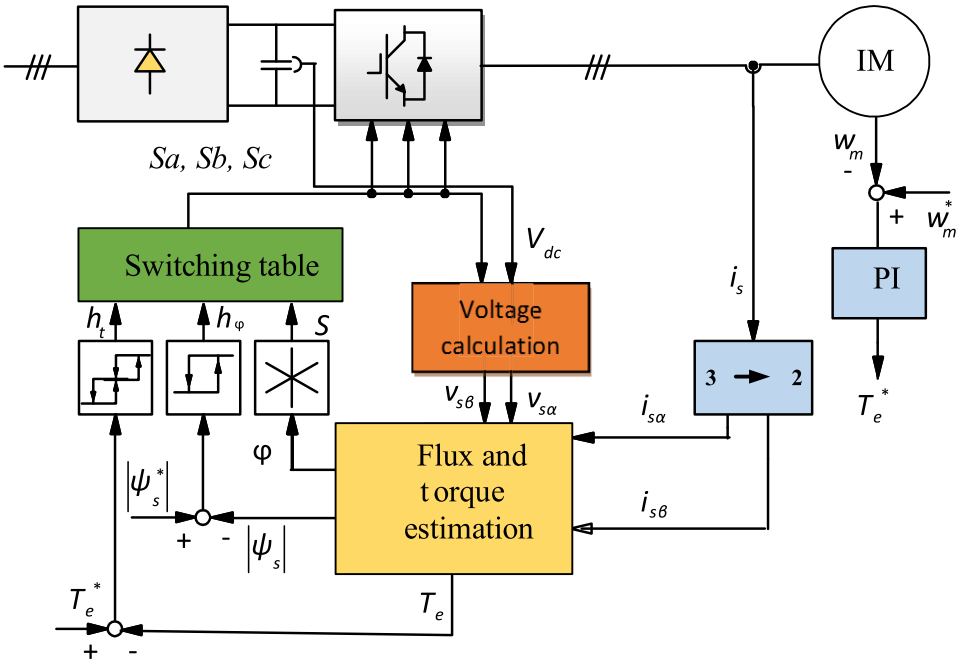

FIGURE 2. The DTC block diagram.

In this paper, the current model is utilized to compute the stator flux. The magnitude of stator flux can be calculated as:

$$|\boldsymbol{\psi}_s| = \sqrt{\boldsymbol{\psi}_{s\alpha}^2 + \boldsymbol{\psi}_{s\beta}^2} \tag{9}$$

The torque is estimated as:

$$T_e = 1.5\, p\, I\, m\, \overrightarrow{\psi_s^*} \cdot \overrightarrow{i_s} \tag{10}$$

As depicted in Fig. 3, the controller of the PI speed produces the torque reference T_e.

The reference value for the stator flux magnitude ($\overrightarrow{\psi_s^*}$) is constant. The basic DTC controller only consists of a three-dimensional lookup table for the h_t torque, the stator flux magnitude h_ψ and for the sector S in which the stator flux angle is situated as demonstrated in Fig. 4.

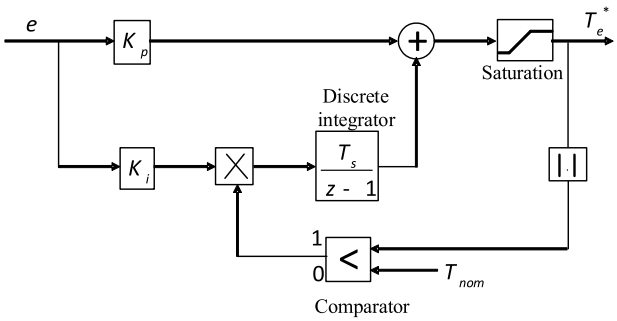

FIGURE 3. The controller of the PI speed with anti-windup.

A. DTC LOOKUP TABLE

The DTC look-up table is demonstrated in Table 2. The sector of the stator flux and the control signals h_t and h_ψ

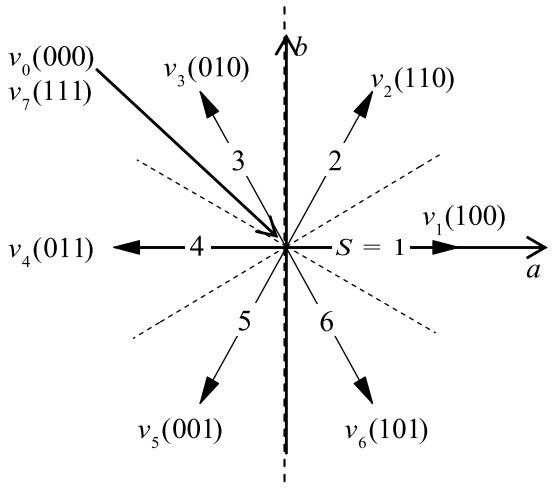

FIGURE 4. Definition of sectors for DTC.

TABLE 2. The look-up table of the DTC voltage vector selection.

Sector	$(h_t \cdot h_\psi)$			
	$(1,1)^{\cdot}$	$(1,-1)^{\cdot}$	$(-1,1)^{\cdot}$	$(-1,-1)^{\cdot}$
1	v_2	v_6	v_3	v_5
2	v_3	v_1	v_4	v_6
3	v_4	v_2	v_5	v_1
4	v_5	v_3	v_6	v_2
5	v_6	v_4	v_1	v_3
6	v_1	v_5	v_2	v_4

are the table inputs which specify the needed excess ("1") or reduction ("−1") of magnitude the stator flux and the torque, respectively.

IV. FINITE CONTROL SET- PREDICTIVE TORQUE CONTROL

The three steps of the FS-PTC scheme are depicted in Fig. 5: flux & torque prediction, flux estimation and cost function optimization.

A. FLUX ESTIMATION

The first stage of the FS-PTC technique is to appreciate the needed variables which cannot be measured. The accuracy of the FS-PTC controller will be directly impacted by the quality of the estimated values. Based on the rotor speed ($\boldsymbol{\omega_m}$) and the stator current measurements, the rotor flux ($\boldsymbol{\psi_r}$) and the stator flux ($\boldsymbol{\psi_s}$) appreciations are designed in PTC [26]. Traditionally, to estimate rotor flux, the rotor current model of IM is typically utilized. Then, the straightforward relationship between rotor and stator flux is employed for estimating stator flux. As a result, the appreciations of the stator and rotor flux is formulated as follows:

$$\frac{d\,\vec{\hat{\psi}}_r}{dt} = R_r \frac{L_m}{L_r}\vec{i}_s - \left(\frac{R_r}{L_r} - j\omega_e\right)\vec{\hat{\psi}}_r \tag{11}$$

$$\vec{\hat{\psi}}_s = \frac{L_m}{L_r}\vec{\hat{\psi}}_r + \sigma L_s \vec{i}_s \tag{12}$$

From backward-Euler approximation the stator and rotor flux are formulated as follows:

$$\vec{\hat{\psi}}_r(k) = \vec{\hat{\psi}}_r(k-1) + T_s\left[R_r\frac{L_m}{L_r}\vec{i}_s k - \left(\frac{R_r}{L_r} - j\omega_e k\right) \times \vec{\hat{\psi}}_r(k-1)\right] \tag{13}$$

$$\vec{\hat{\psi}}_s(k) = \left[\frac{L_m}{L_r}\vec{\hat{\psi}}_r(k) + \sigma L_s\,\vec{i_s}(k)\right] \tag{14}$$

The appreciated electromagnetic torque is formulated as follows:

$$\hat{T_e}k = 1.5\,p\,I\,m\,\vec{\hat{\psi}}^{*}_{s}k\,\vec{i_s}(k) \tag{15}$$

The stator flux and the electromagnetic torque are the PTC control variables, and behavior prediction is required at the sampling step $(k+1)$. In overall, the IM stator voltage model is employed to predict stator flux and can be written as follows in discrete time steps:

$$\vec{\psi}^{p}_{s}(k+1) = \vec{\hat{\psi}}_s k + T_s\vec{v}_s(k) - T_s R_s \vec{i}_s k \tag{16}$$

Stator current is forecasted to anticipate the electromagnetic torque. Consequently, the stator current and torque predictions are as follows:

$$\vec{i}^{p}_{s}(k+1) = \left(1 + \frac{T_s}{\tau_\sigma}\right)\vec{i}_s(k) + \frac{T_s}{\tau_\sigma + T_s} \times \left\{\frac{1}{R_\sigma}\left[\left(\frac{k_r}{\tau_r} - k_r j\omega_e k\right)\vec{\hat{\psi}}_r(k) + \vec{v}_s(k)\right]\right\} \tag{17}$$

$$T^{p}_{e}(k+1) = 1.5\,p\,I\,m\,\vec{\hat{\psi}}^{p}_{S}(k+1) * \vec{i}^{p}_{S}(k+1) \tag{18}$$

As the rotor time constant is more major than the sampling time and the rotor flux travels so slowly compared with the stator flux, it is typical to make this assumption $\omega(k) = \omega(k+1)$ and $\vec{\psi}_r(k) = \vec{\psi}_r(k+1)$, respectively [27].

In electro-optical/infrared systems, torque ripple can compromise visual data quality, affecting targeting accuracy in an offensive application or even compromising soldier safety in a defensive application. In television applications, torque ripple directly affects image resolution and clarity. Also, With the gradual improvement of the comfort and stability requirements of the passenger car, the vibration and noise of the drive motor for the electric vehicle and torque ripple impact and other indicators affecting the comfort of the vehicle.

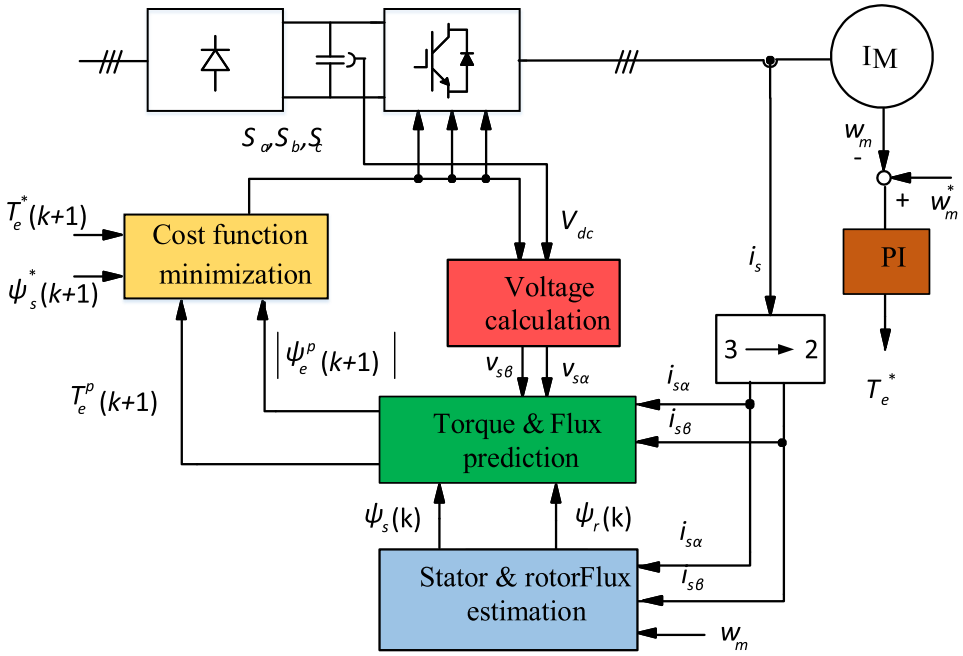

FIGURE 5. Block diagram of PTC.

B. COST FUNCTION OPTIMIZATION

In power converters and drives, the control effort is related with the voltage or current variations, the switching frequency or the switching losses. Using FS-PTC, it is possible to consider some variations in the cost function, in order to reduce control effort. These variations are classified in three groups: implementation of switching schemes, input constraints and output constraints. The main idea is to minimize the switching frequency but without increase significantly the THD of current and torque. For this reason, a tradeoff between switching frequency and THD is required. The second variation to the cost function is the inclusion of input constraints. In the literature, two different input constraints are considered. In order to consider in the cost function, the reduction of the number of commutations, a simple approach is to include a term in the cost function that is the number of switches that change when the next voltage vector is applied, with respect to the previously applied switching state. The function takes a large value when the predicted currents exceed a given limit, acting in practice as constraints on the current magnitudes. Finally, the current limitation is only required when weighting factors are not adjusted.

Typically, the cost function in FS-PTC includes flux and torque error absolute values. Consequently, the cost function is described as [28]:

$$j = \left|T_e^*(k+1) - T_e^p(k+1)\right| + \lambda_p ||\psi_o^*| - |\psi^p(k+1)|| \tag{19}$$

As the sampling time is extremely brief, it is customary to presume that $T_e^*(K+1) = T_e^*(K)$. A switching transition term is incorporated in the cost function to lower the average switching frequency and can be defined as [29]:

$$h_{sw} = \sum_{x=a,b,o} \left|S_x(k+1)_i\right| - S_x(k) \tag{20}$$

The FS-PTC with switching transition term in the cost function is described as FS-PTC f_{sw}. The cost function (j) must comprise other term I_m which is created depending on the extreme stator winding current capacity to prohibit over-current. Therefore, the term I_m can be describe as:

$$I_m = \begin{cases} \infty, & if \left|\vec{i}_s^p(k+1)\right| > I_{max} \\ 0, & therwise \end{cases} \tag{21}$$

The cost function j for the controller can be formulated as follows:

$$j = \left|T_e^*(k+1) - T_e^p(k+1)\right| + \lambda_p ||\vec{\psi}_s^*| - |\vec{\psi}_s^p(k+1)|| + \lambda_n h_{sw} + I_m \tag{22}$$

The fourth term, I_m without the requirement for a weighting factor. The optimum voltage vector (v_{opt}), which allow the minimum value of j, will be chosen and exercised to the motor by the inverter at the following sampling instant. The calculation of a control technique's time creates a one-step time delay that needs to be compensated for in a real-time implementation. It is accomplished by two steps forecast. The forecasted stator flux $\vec{\psi}_s^p(k+1)$ from (16) and the stator current $\vec{i}_s^p(k+1)$ from (17) are utilized as the initial states for the forecasts at time instant $k+2$. To foretell the values of the $\vec{\psi}_s^p(k+1)$ and the $\vec{i}_s^p(k+1)$, the optimum voltage vector $v_{opt}(k)$ used to the motor at instant k is employed in (16) and (17), respectively. Therefore, for delay compensation is

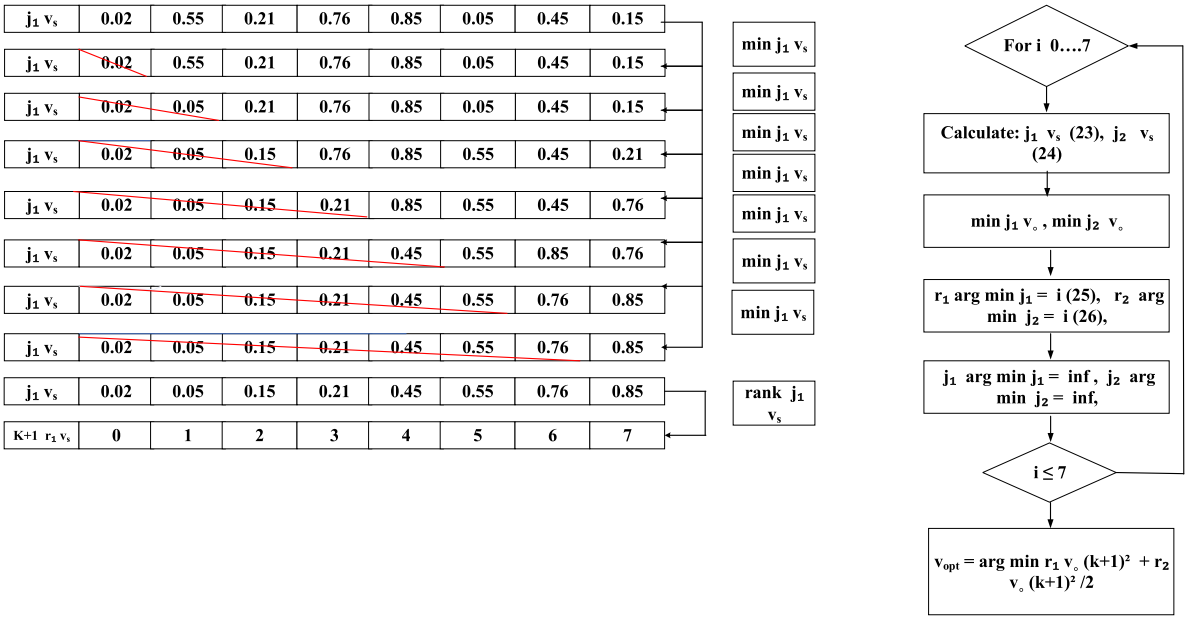

FIGURE 6. The ranking strategy steps.

TABLE 3. Example of voltage vector selection.

v_s	$j_1 v_s$	$j_2 v_s$	$r_1\ v_s$	$r_2\ v_s$	$\frac{(r_1\ v_s\ k+1)+(r_2\ v_s\ k+1}{2}$	$\frac{(r_1\ v_s\ k+1)^2+(r_2\ v_s\ k+1)^2}{2}$
v_0	0.02	0.74	0	7	3.5	24.5
v_1	0.55	0.12	5	2	3.5	14.5
v_2	0.21	0.06	3	1	2	5
v_3	0.76	0.14	6	3	4.5	22.5
v_4	0.85	0.01	7	0	3.5	24.5
v_5	0.05	0.23	1	4	2.5	8.5
v_6	0.45	0.35	4	5	4.5	20.5
v_7	0.15	0.66	2	6	4	20

implemented, by reducing the next cost function, the optimal voltage vector is chosen [30].

$$j = \left|T_e^*\ (k+2) - T_e^p\ (k+2)\right| + \lambda_p||\vec{\psi}_s^*| - |\vec{\psi}_s^p\ (k+2)\ || + \lambda_n h_{sw} + I_m \quad (23)$$

C. WEIGHTING FACTORS ELIMINATION

In the proposed method, the weighting factor tuning is replaced by a multi-objective ranking based approach, and weighting factor calculation is avoided. The method is based on the idea that the selected voltage vector should allow a fair minimization of all the objective functions. In fact, in multi-objective ranking-based FS-PTC the obtained fitness value of stator flux and torque are similar, while in conventional FS-PTC they values are different and weighting-factor dependent. However, if more weight is assigned to the flux using the conventional approach the fitness value will be similar with the proposed FS-PTC approach. Finally, the major advantage of this proposed alternative is the full tuning-process elimination of inner control-loop parameters.

In conventional FS-PTC scheme, the controller tries to minimize the cost functions for each particular objective, minimizing an aggregate objective function (AOF) composed by a linear combination of them. Multi-objective optimization strategy is proposed to replace the AOF by a multi-objective optimization stage allowing a fair optimization of the required control objectives. The method is based in a technique applied to the ranking of populations in evaluative optimization algorithms based on genetic algorithms, but it is simplified significantly since the possible solutions is a finite control set.

The choice of value λ_p is a challenging undertaking, and it has a major impact on the controller performance. To address this issue, the weighting factor λ_p should be eliminated. The proposed method used two different cost functions to address the issue of voltage vector choosing in conventional PTC which can be described as follows:

$$j_1 = \left|T_e^*(k+2) - T_e^p(k+2)\right| \tag{24}$$

$$j_2 = \left|\left|\vec{\psi}_s^*\right| - \left|\vec{\psi}_s^p(k+2)\right|\right| \tag{25}$$

where j_1 and j_2 are the errors of the torque and stator flux, respectively. This simultaneous optimization can be interpreted as a vector optimum problem. The proposed multi objective ranking-based strategy evaluates these components separately for each possible voltage vector of the converter. The operation of the Multi-objective Ranking-based FS-PTC strategy is as follows:

First, the values obtained from the evaluation of each objective function,, are sorted. Then, a ranking value is assigned to each error value. Voltage vectors $j_1 v_s\,(k+1)$ and $j_2 v_s\,(k+1)$ with lower error are assigned a lower ranking, however voltage vectors with higher error are getting a higher ranking as follows:

$$j_1 v_s\,(k+1) \rightarrow r_1 v_s\,(k+1) \tag{26}$$

$$j_2 v_s\,(k+2) \rightarrow r_2 v_s\,(k+2) \tag{27}$$

where $r_1 v_s(k+1)$ and $r_2 v_s(k+1)$ are the ranking values related with j1 and 2, respectively. The proposed ranking technique can be explained in the sequence below in Fig. 6. The ranking value determines the relative quality of each possible voltage vector with respect to all the remaining possibilities. The associated ranking value is a dimensionless variable, while the error has a specific dimension. By selecting the ranking with the lowest value, it is possible to select an optimal voltage vector, from the point of view of one variable error. On the other hand, by selecting the ranking with the lowest value, it is possible to select an optimal voltage vector, from the flux error point of view.

Now, to select which one is the best overall voltage vector within these alternatives, an average criterion is used in which the voltage vector with the minimum average value of its rankings is selected, resulting in an equal compromise of tracking for both variables, torque, and flux. Then, the proposed optimization based on average ranking is given as:

$$v_{opt} = arg\,min\frac{(r_1 v_s\,(k+1))^2 + (r_2 v_s\,(k+2))^2}{2} \tag{28}$$

The sorting of the possible solutions according to an associated ranking is explained. Here, a recursive quicksort algorithm is used. The quicksort algorithm is a divide-and-conquer algorithm. It first divides the list to be sorted into two smaller sublists: the low elements and the high elements. Then, the algorithm can recursively sort the sublists. The quicksort algorithm used can be described in the following sequence.

TABLE 4. The IM parameters.

$P_n = 3\ kW$	$I_n = 6.3\ A$
$R_s = 2.3\Omega$	$\psi_{snom} = 0.8\ Wb$
$R_r = 1.8\Omega$	$T_{nom} = 20Nm$
$L_s = 0.261H$	$p = 2$
$L_r = 0.261H$	$J = 0.03Kgm^2$
$L_m = 0.258H$	$\omega_n = 1415rpm$
$f = 0.0003$	$Ts = 80\mu s$

Step 1 Pivot: Select an element from the list (called a pivot).

Step 2 Partition: Reorder the list so that all elements with values less than the pivot come before the pivot. Elements with values greater than the pivot come after it. Then, the pivot is in its final position.

Step 3 Sort 1: Recursively sort the sublist of lesser elements.

Step 4 Sort 2: Recursively sort the sublist of greater elements. The algorithm is implemented using recursive functions written in C code.

To explain the proposed technique, an example is given in Table 3. The torque error is obtained by the voltage v_0 is $j_1 v_0 = 0.02$, the assigned ranking value is $r_1 v_0 = 0$ because it is the lower error value, while the torque error is obtained by the voltage v_4 is $j_1\ v_4 = 0.85$ and then, the ranking assigned is $r_1\ v_4 = 7$ because it is the higher error value. The same procedure should be executed for the flux errors with their respective ranking assignation r_2. It is possible for some voltage vectors have the same ranking. To address this problem, the optimization presented in (28) is selected.

The voltage v_2 vector gives the fewer value of the rankings $r_1 = 3$ and $r_2 = 1$. Finally, the voltage vector should be applied in the next sampling time is v_2.

V. IMPLEMENTATION AND RESULTS

A. SIMULATION RESULTS

In a MATLAB/Simulink program, the model contains an Embedded MATLAB Function block with four input (speed, torque, flux, current) and three output (Sa, Sb, Sc). The Embedded MATLAB function calls a custom C function to sort the values obtained from the evaluation of each objective function. The Embedded MATLAB function calls a C function that uses a custom C header file and eml.ceval instruction. a simulated comparison is carried out to confirm the efficacy of the two techniques. traditional testing was used to determine the properties of the IM, which are presented in Table 4.

The PI controllers of speed are set up with the same parameters to allow for a fair comparison of the two techniques. In both the test bench and the simulation, the sampling time has been adjusted to be $80\mu s$. Simulink in

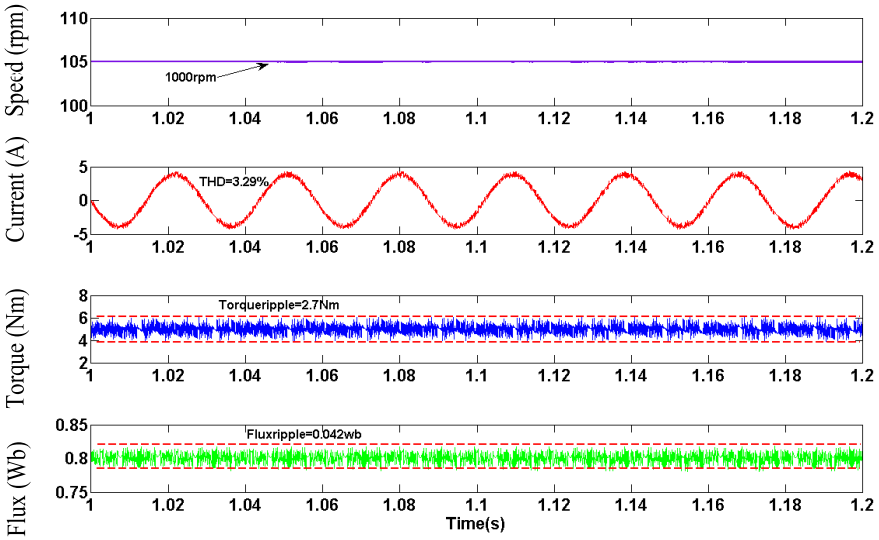

(a) The proposed FS-PTC.

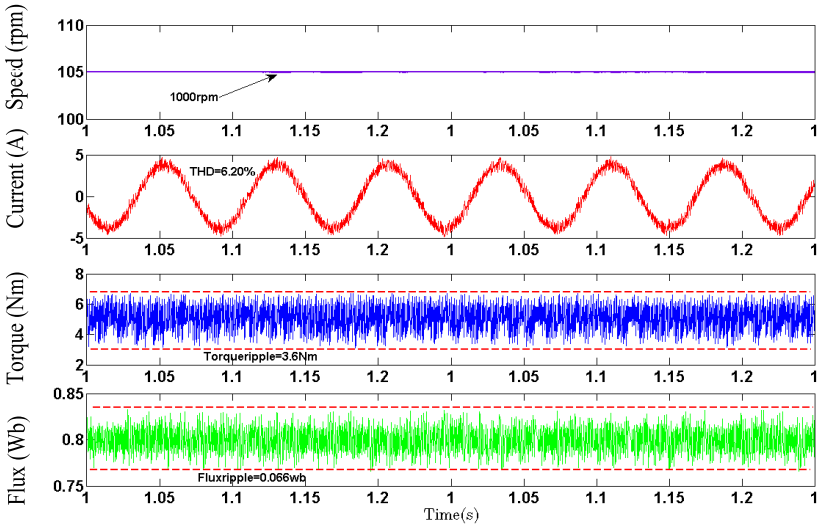

(b) The conventional DTC.

FIGURE 7. The steady state simulation results by application (a) The proposed FS-PTC, (b) The conventional DTC.

MATLAB was employed for building the simulation model of the system. In the first simulation, the FS-PTC and traditional DTC steady-state behaviour are shown when the machine is running at 1000 rpm and 25% of the load torque (5 Nm). Fig. 7 (a) and Fig. 7 (b) for both techniques indicate the stator flux, the speed, the torque, and the stator current at the steady state, respectively. The stator flux reference is the nominal value (0.8Wb). The results demonstrate that the FS-PTC outperforms the standard DTC, particularly due to the significant decreasing the flux ripples and the torque that results in a sinusoidal current waveform. The second case of the simulation demonstrates a speed-reversal running from 1000 to −1000 rpm. the speed dynamics, the stator flux, the produced, torque, and stator current for each technique are shown in Figs. 8(a) and Fig. 8(b), respectively. The results indicate that the FS-PTC produces a superior dynamic performance than the traditional DTC. However, both techniques result in a separate control of the stator flux and the produced torque.

Fig. 9 shows the flux components dynamics, magnitude of the stator flux and the flux track for both methods, respectively. According to Fig. 9, the obtained results by application of the proposed technique are superior compared with the traditional technique in terms of flux and torque ripple reduction.

B. EXPERIMENTAL RESULTS

On an experimental platform, the FS-PTC and DTC techniques have both been tested. The experimental setup is demonstrated in Fig. 11. It comprises squirrel-cage IM driven by an IGBT depended on two level-VSI. The motor shaft is coupled to a permanent magnet synchronous machine

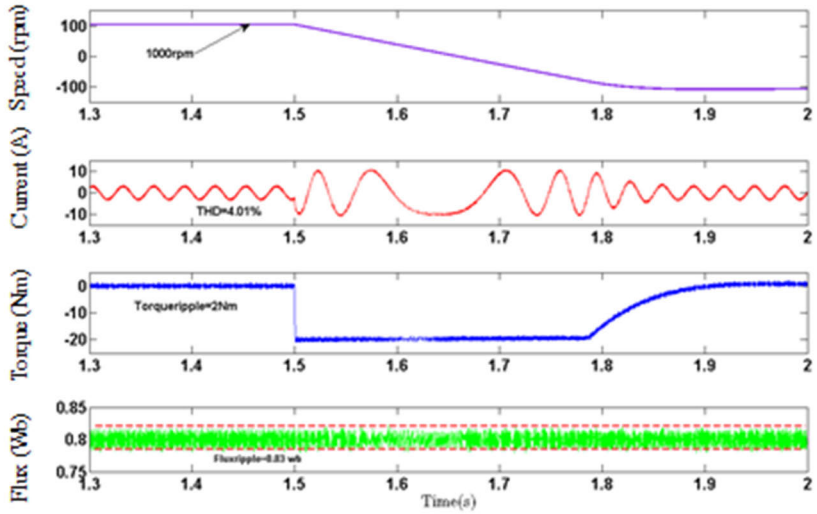

(a) The proposed FS-PTC.

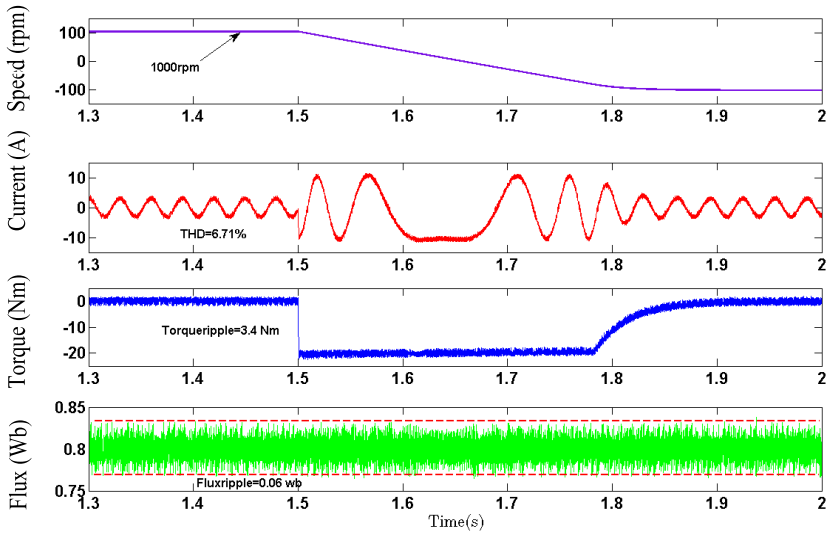

(b) DTC Conventional.

FIGURE 8. The speed reversal maneuver simulation results (from 1000 rpm −1000 rpm) by (a) The proposed FS-PTC, (b) The conventional DTC.

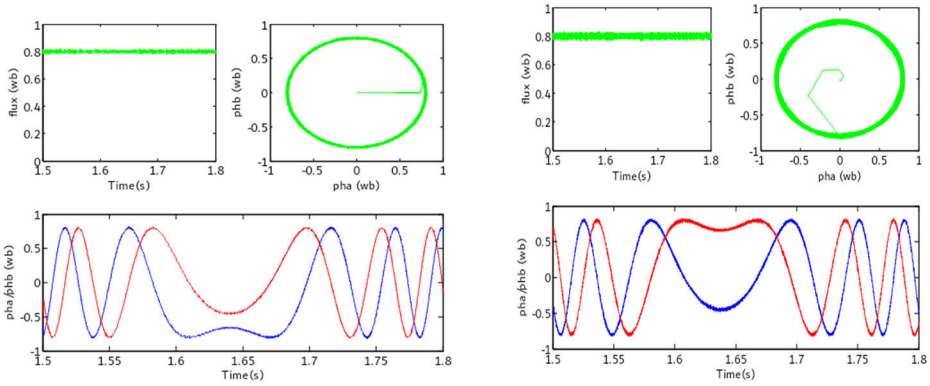

FIGURE 9. Simulation results for a speed reversal maneuver.

(PMSM), which serves as a load. To adjust the load, a rheostat is connected in series with the PMSM's armature. The motor shaft also has an incremental encoder to measure speed. The control platform used is a dSPACE DS1104

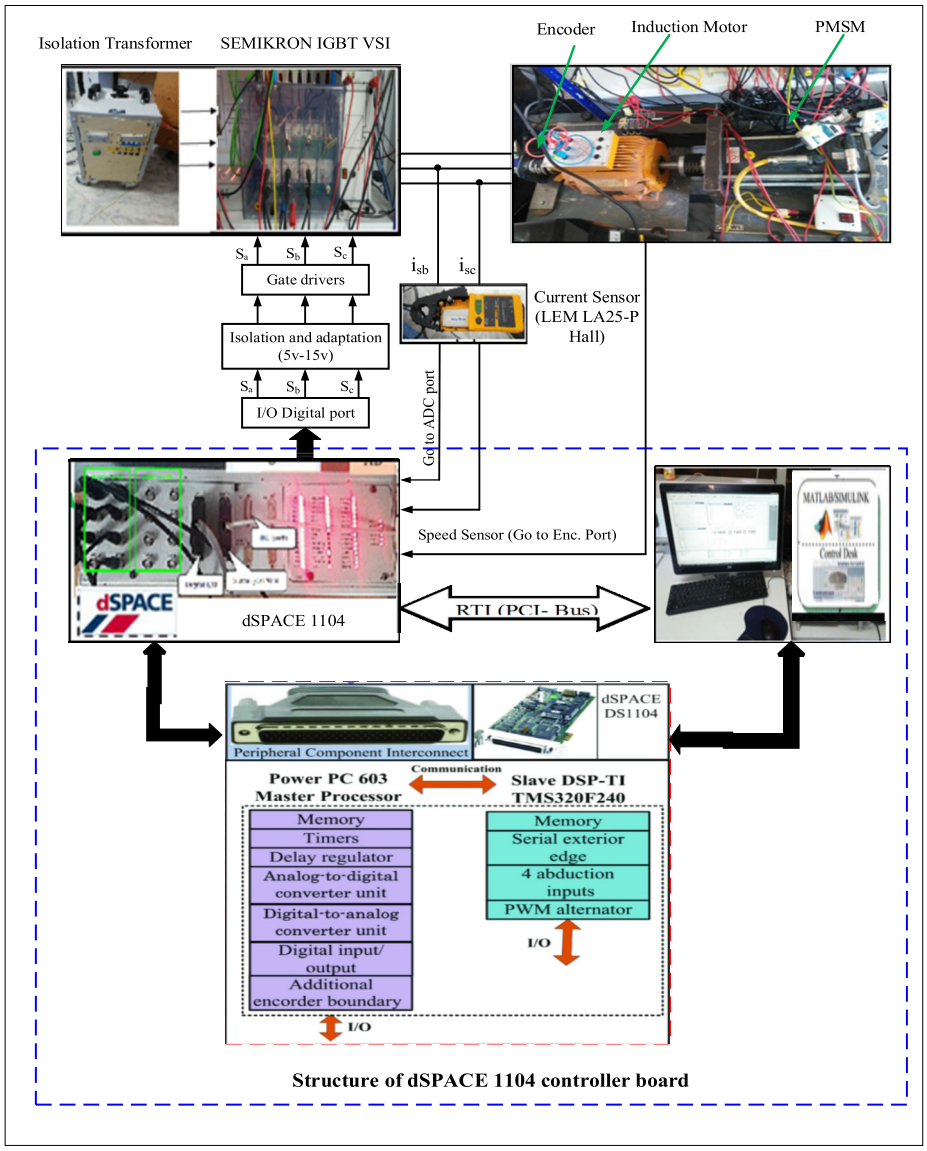

FIGURE 10. Real–time simulator architecture of the system.

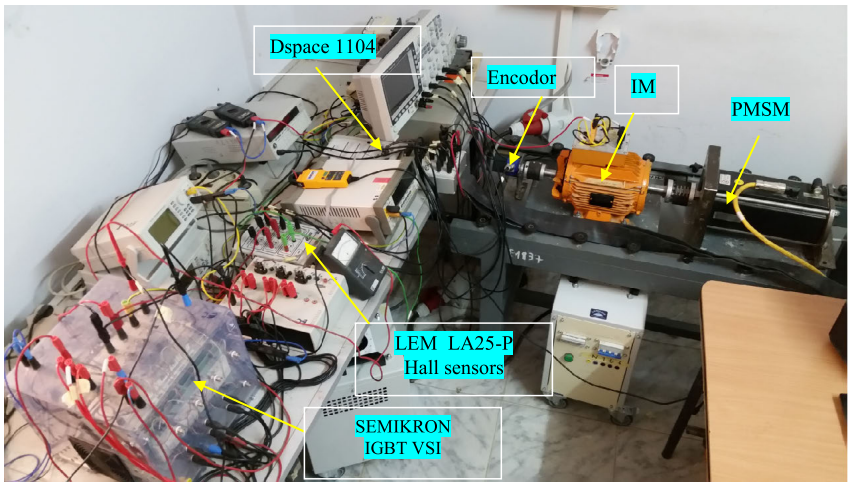

FIGURE 11. Experimental setup.

TABLE 5. The PMSM and the controller parameters.

Control setting values	PMSM parameters
$K_p = 0.4, K_i = 10\ \lambda_p = 100, \lambda_n = 0.05\ I_{max} = 15A, h_t = 0.1, h_\psi = 0.01$	$P = 4kW,$ $V = 400V,$ $I_a = 11A,$ $\omega = 3000rpm$

R&D. The control strategies are programmed in C, while the Human Machine Interface (HMI) is programmed using Control Desk software. The system has a primary processor for calculations, model PowerPC processor MPC8240 and another slave processor for data transmission and peripheral control, model DSP Texas Instruments TMS320F240. The system is connected to a desktop computer through a PCI slot. The control panel unit allows the connection of input and output signals, both analog and digital encoders.

The six gate signals are transmitted from dSPACE through I/O boards. The I/O board is connected on digital I/O dSPACE port. The I/O board is fed by the control platform, but they can be externally supplied when more I/Os are required. The connection pins and software trips are Port (IO 0, IO3, IO, IO4, IO6, IO8, IO10) as shown in Fig. 10. The implemented HMI is developed using the software of dSPACE Control Desk 3.7. The execution time is measured with the dSPACE profiler. The proposed algorithm requires additional calculations for multi-objective method (calculations not used in the conventional FS-PTC). However, the calculations are very simple. Therefore, the required maximum execution time is 75.6 μs. Most of the execution time is spent on the estimations (Torque and flux) and predictions: 27% and 62%, respectively. For this reason, it is possible to execute the proposed control algorithm within 80 μs. Table 5 lists the controllers and the IM parameters.

The suggested FS-PTC performances without weighting factor are evaluated with and without including the switching transition term in the cost function and compared with the traditional DTC for different study cases which can be presented as follows:

The effectiveness of the proposed FS-PTC in terms of torque and flux ripple, stator current THD, and average switching frequency of the inverter is tested. The performance is compared to the FS-PTC strategy without weighting factor including the switching transition term in the cost function. A comparative analysis at a particular operating point is then conducted with the well-established FS-PTC without including the switching transition term and DTC strategies. The effectiveness of the proposed FS-PTC without weighting factor is investigated for the followings:

a) steady-state behavior at medium- and low-speed operations;

b) transient capability of the FS-PTC under speed (rated) reversal;

c) robustness against an external rated-load torque disturbance;

d) average switching frequency.

e) weighting factor elimination.

1) CASE 1: THE SYSTEM PERFORMANCE UNDER RATED SPEED REVERSAL

In this case the system performance is studied at reverse speed under 5 Nm load torque and 1000 rpm with application the suggested FS-PTC system without a weighting factor at is implemented the FS-PTC f_{sw} and the conventional DTC. Fig. 12 shows the system performance FS-PTC including the stator flux, the stator current, the stator flux, the torque and the speed with application the suggested FS-PTC without weighting factor, the FS-PTC f_{sw} and the conventional DTC. According to Fig. 12, well performance can be obtained with application of the suggested FS-PTC without weighting factor compared to the conventional DTC control method where the oscillation of the stator current is low and there is no overshooting in the rotor speed as well as the ripple in the torque is low. In this case, the THD with application the suggested FS-PTC, the FS-PTC f_{sw} and the conventional DTC are 4.75%, 4.95%, and 6.92%, respectively. Thus, the minimum THD is obtained by application the suggested FS-PTC compared to the other methods. In addition to that, the average switching frequencies with application the suggested FS-PTC, the FS-PTC f_{sw}, and the conventional DTC are 2.98 kHz, 3.43 kHz, and 4.3 kHz; respectively.

2) CASE 2: THE SYSTEM PERFORMANCE AT THE STEADY STATE CONDITION UNDER LOW AND MEDIUM SPEED OPERATION

In this case, the suggested FS-PTC without weighting factor performance is depicted at the steady state condition where the speed reference and the load torque are adjusted to be 1000 rpm and 5 Nm, respectively. Fig. 13 shows the system performance with application the suggested FS-PTC, the FS-PTC f_{sw}, and the conventional DTC. Judging from Fig. 13, the torque ripple is the lowest with application the suggested FS-PTC without weighting factor compared to the FS-PTC f_{sw} and the conventional DTC.

The stator current frequency spectrum for this case with application of the suggested FS-PTC, the FS-PTC f_{sw}, and the conventional DTC are depicted in Fig. 14(a), Fig. 14(b) and Fig. 14(c); respectively. According to Fig. 14, the proposed FS-PTC is superior compared to the other methods in terms of the switching frequency variations where the average switching frequency (f_{sw}) that obtained by the suggested FS-PTC without weighting factor is the lower value (3.43 kHz) compared to the obtained by the conventional DTC (4.3 kHz). The frequency spectrum of the stator current is presented in Fig. 14(b) with an average switching frequency equal to 2.98 kHz. The frequency spectrum of the stator current for the traditional DTC is presented in Fig. 14(c) with an average

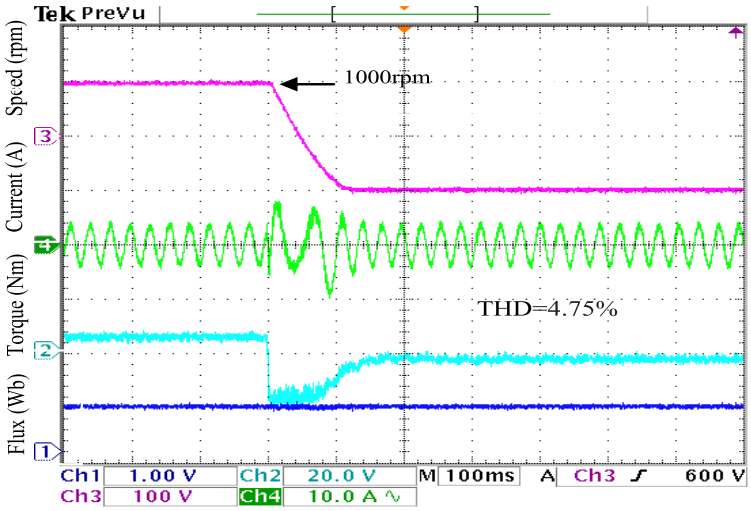

(a) FS-PTC without weighting factor.

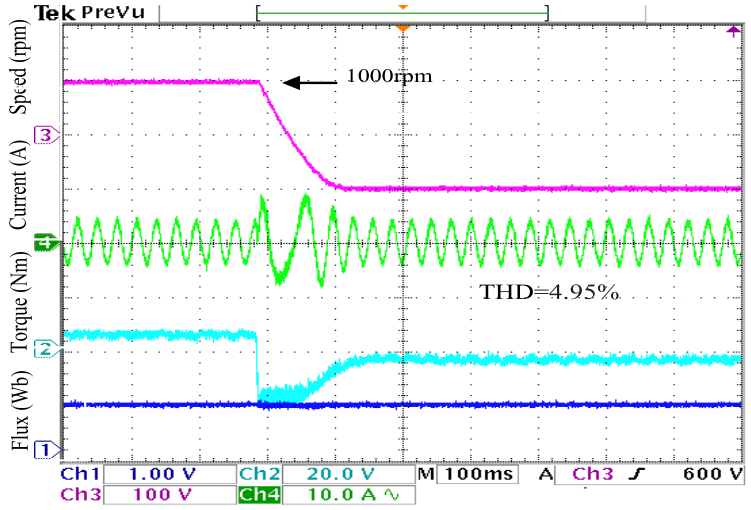

(b) The FS-PTC (f_{sw}).

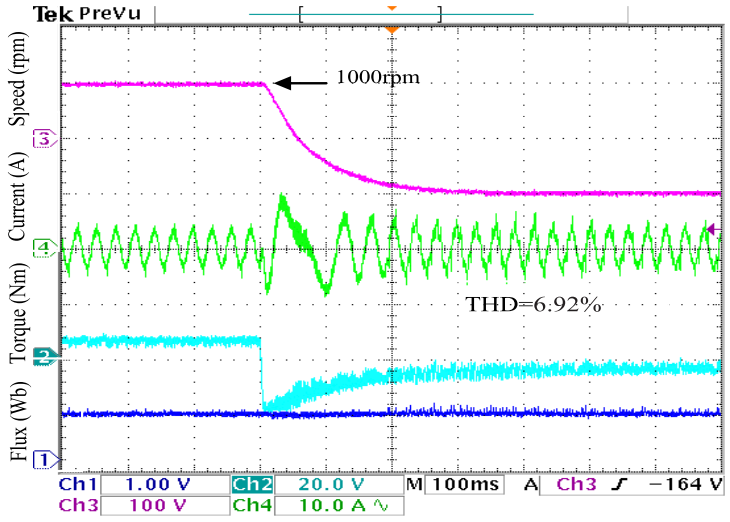

(c) Conventional DTC.

FIGURE 12. Experimental results for case 1.

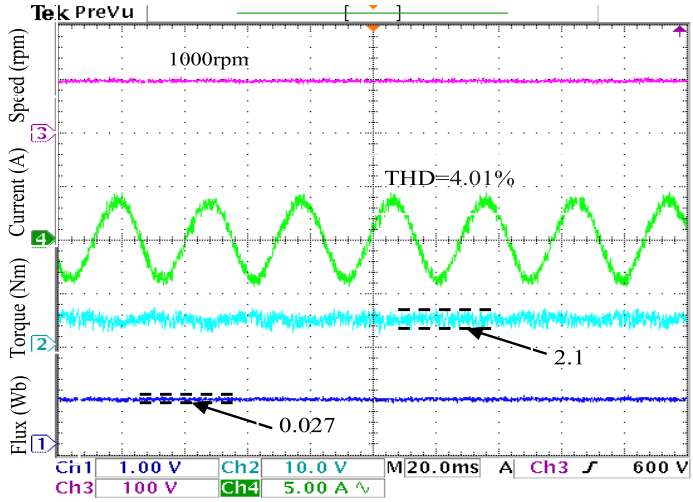

(a) The FS-PTC without weighting factor.

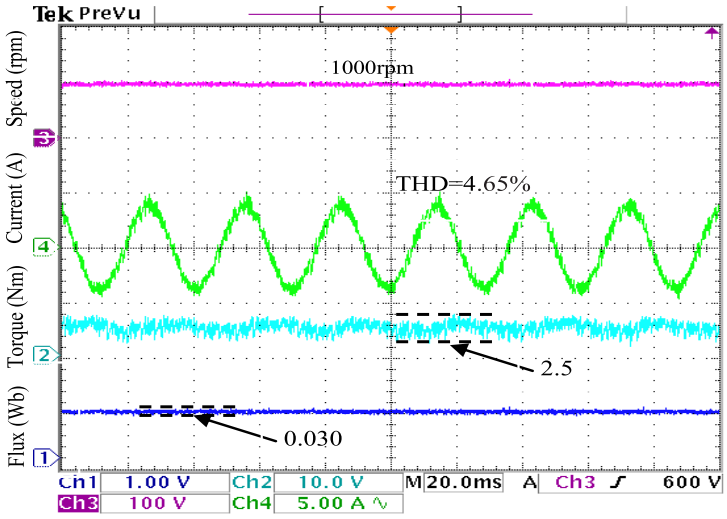

(b) The FS-PTC (f_{sw}).

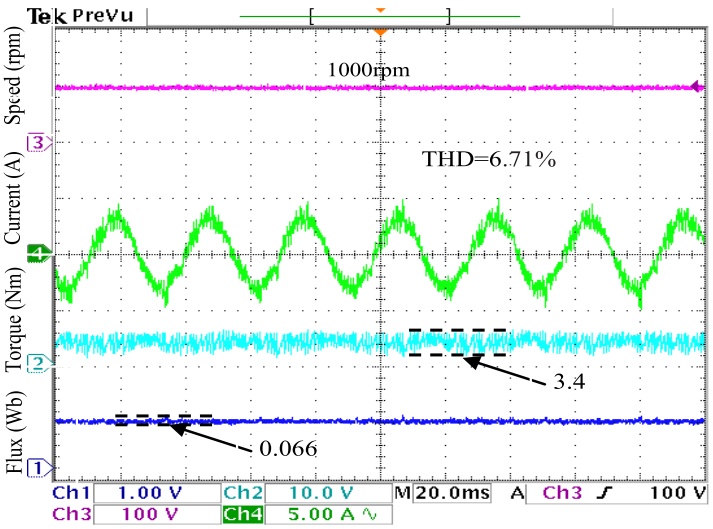

(c) The conventional DTC.

FIGURE 13. Experimental results for case 2.

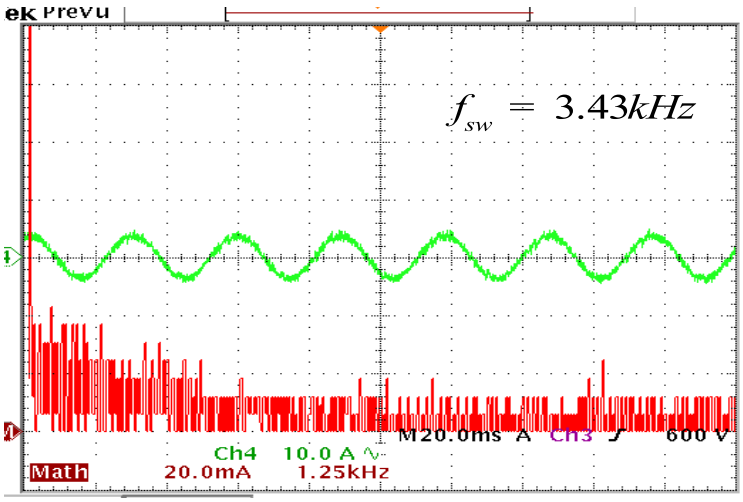

(a) The FS-PTC without weighting factor

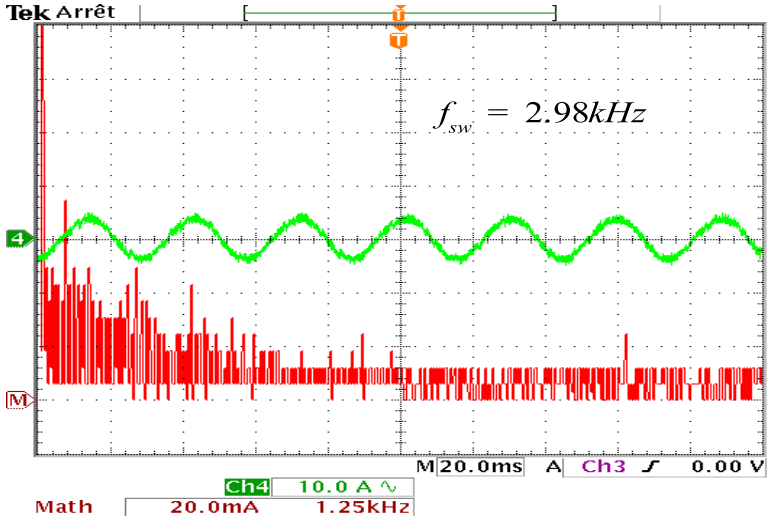

(b) The FS-PTC (f_{sw}).

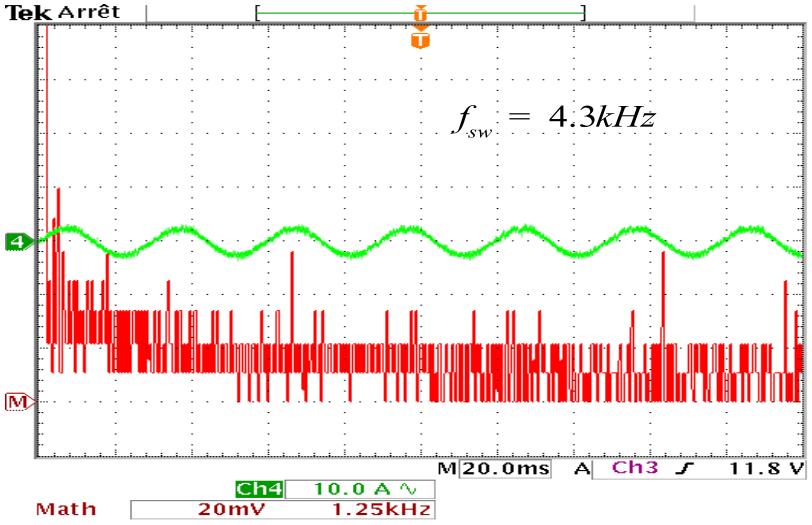

(c) The conventional DTC.

FIGURE 14. experimental frequency spectrum of the stator current for case 2.

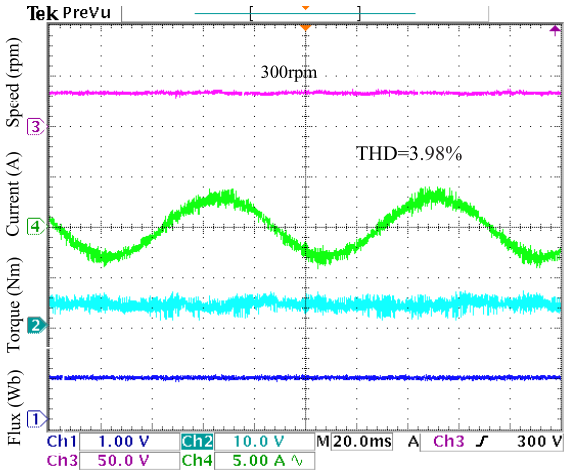

(a) The FS-PTC (without weighting factor)

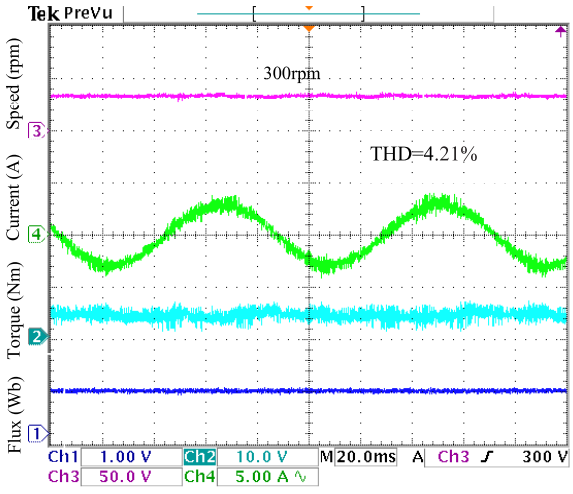

(b) The FS-PTC (f_{sw}).

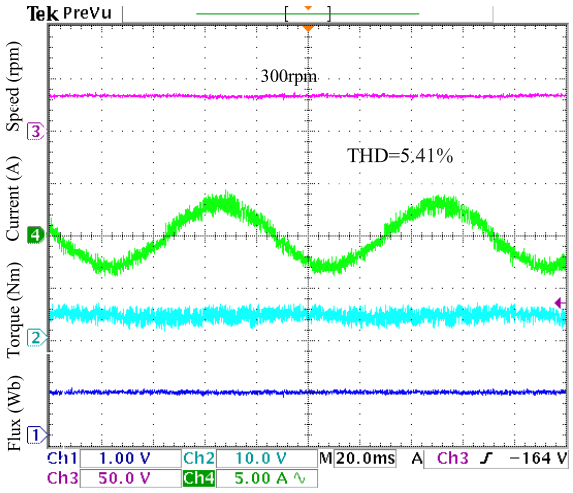

(c) The conventional DTC

FIGURE 15. Experimental steady-state results.

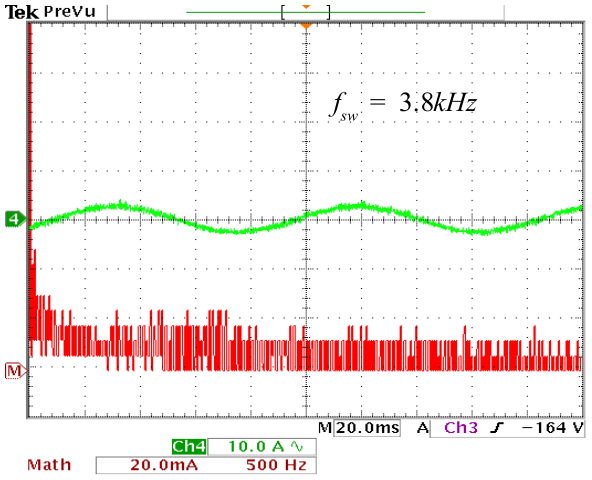

(a) FS-PTC without weighting factor

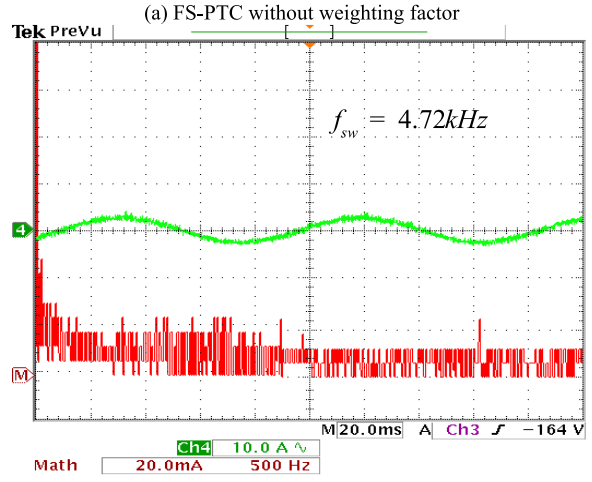

(b) The FS-PTC (f_{sw}).

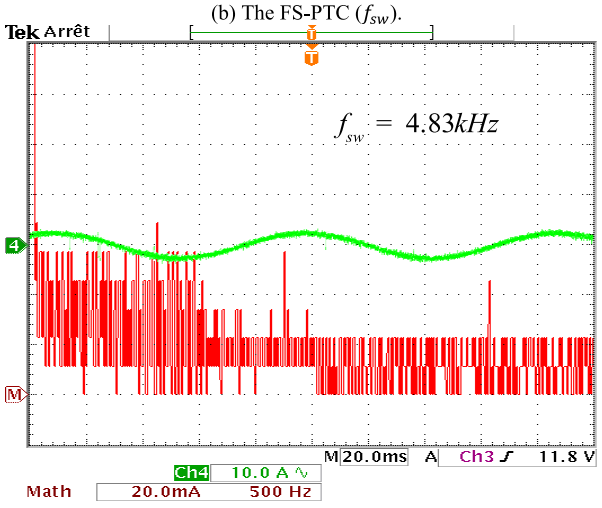

(c) Conventional DTC

FIGURE 16. The stator current frequency spectra at 300 rpm and load torque of 5 Nm.

switching frequency equal to 4.3 kHz. The torque ripples increase as more weight is enjoined on the switching transition term to further lower the average switching frequency. for this reason, proper choosing of weighting factors is a combination task. Table 6 provides a comparison of the steady-state performances. The experimental results that obtained by application the suggested FS-PTC, the FS-PTC f_{sw}, and the conventional DTC. A switching transition term is added to the cost function to lower the average switching

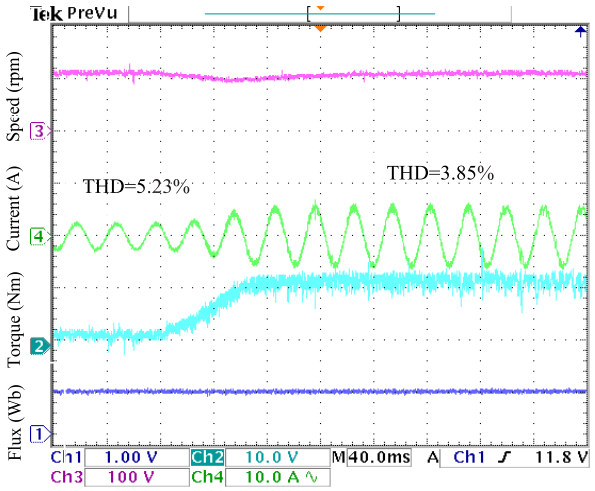

(a) FS-PTC (without weighting factor).

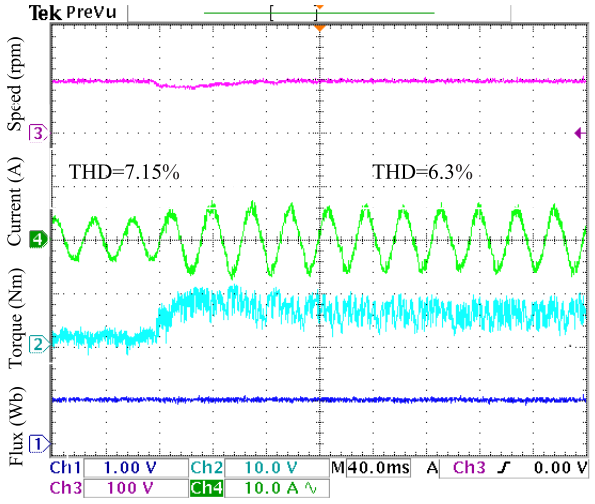

(b) The conventional DTC.

FIGURE 17. Experimental response from 0 Nm to 10 Nm load disturbance at 1000 rpm.

frequency of the proposed FS-PTC. Then a weighting factor is enjoined to the frequency term, as long as the torque and flux ripples are nearly identical. Based on the Table, the torque ripple is the lowest with application the suggested FS-PTC without weighting factor compared to the FS-PTC f_{sw} and the conventional DTC. Also, it is superior compared to the other methods in terms of the switching frequency variations where the average switching frequency (f_{sw}) that obtained by the suggested FS-PTC without weighting factor is the lower value (3.43 kHz) compared to the obtained by the conventional DTC (4.3 kHz). The FS-PTC has the lowest flux ripple when compared with the other methods. Consequently, the FS-PTC is the best solution of system and the control performance is enhanced considerably.

To test the low-speed performance, the machine is running at 300 rpm with load torque of 5 Nm. The results are demonstrated in Fig. 15 (a), (b) and (c).

TABLE 6. Comparison of DTC and suggested FS-PTC: $w_m = 1000rpm$, $T_L = 5N.m$, $T_o = 80\mu s$.

Index	Conventionne l DTC	$FS-PTC$	$FS-PTC\ f_{sw}$
THD	6.71%	4.01%	4.65%
Torque ripple	4.3	2.1	2.5
Flux ripple	0.066	0.027	0.030
Average Switching frequency (f_{sw})	4.3 kHz	3.43 kHz	2.98 kHz

In case of application the FS-PTC without weighting factor, the stator current THD is 3.98% while this value is reduced to with application FS-PTC f_{sw} with average switching frequency and the conventional DTC 4.21% and 5.41%, respectively which verifies the effectiveness of the proposed FS-PTC without weighting factor compared to other methods. The stator current frequency spectra of the FS-PTC without weighting factor, the FS-PTC f_{sw} and the conventional DTC are provided in Figs. 16(a), 16(b) and 16(c), respectively. According to Figure 16, at low speed, the FS-PTC f_{sw} reduction in average switching frequency is low compared to its performance at high speed. In this case, the average switching frequency values with application the FS-PTC, the FS-PTC f_{sw} and the conventional DTC are 3.8 kHz, 4.72 and 4.83 kHz, respectively. At low speeds, the torque and flux ripples occur, and thus there is no improvement in the average switching frequency.

3) CASE 3: THE SYSTEM PERFORMANCE AT EXTERNAL LOAD DISTURBANCE

In this case, the system performance is studies at load disturbance with application the FS-PTC and the classical DTC. Fig. 17(a) illustrates the variations of the flux, torque, speed and current with application the proposed FS-PTC while Fig. 17(b) depicts variations of the flux, torque, speed and current with application the traditional DTC. In this case, the load is changed from 0 Nm to 10 Nm at 1000 rpm. Judging from these Figures, the speeds track their reference rabidly at load disturbance and there is no variation in flux from its rated value which entirely guarantees separate control of flux and torque. In addition to that the stator currents' THD is 5.23 % before and after load disturbance still is not changed in case of using the proposed FS-PTC while in case of implementation the classical DTC the stator currents' THD was varied from 6.3% and 7.15% before and after load disturbance, respectively.

VI. CONCLUSION

This article develops and experimentally tests an induction motor drive based on FS-PTC without weighting factors. The

controller offers rapidly dynamic responses when compared to the classical DTC technique. The main feature of the proposed technique is simpler in structure compared with traditional DTC. A switching transition term is comprised of the cost function for average switching frequency decrease. This advanced method ameliorates the performance of the traditional DTC, especially the reduction of flux and torque ripples, and reducing of the switching frequency. The experimental and simulation findings demonstrate that the inverter's switching frequency is decreased with application of the proposed FS-PTC technique, and the control performance is enhanced considerably.

APPENDIX
PROOF

The drive considers a cascade control loop, composed by a non-linear internal controller and an external PI speed controller, where the speed control loop bandwidth is lower than the inner loop. Remember that speed is a mechanical variable, it is slower than electrical variables. Furthermore, FS-PTC has a high bandwidth allowing a high decoupling degree between inner and outer loop. The conception of the PI controller is based on the compensation of its time constant with the one of the processes of the variable to be controlled. The block diagram of the PI control is presented in Fig. 18.

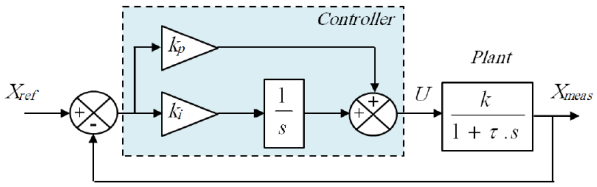

FIGURE 18. The block diagram of the PI control.

The form of the PI controller is:

$$C(s) = k_p + \frac{k_i}{s} \tag{29}$$

The transfer function of the plant controlled by this PI controller is:

$$H(s) = \frac{k}{1+\tau s} \tag{30}$$

where, $\tau = \frac{J}{f}$ and $k = \frac{1}{f}$

The open loop transfer function of the global system is given by:

$$H_{ol}(s) = kk_i \frac{1+\frac{k_p}{k_i}s}{s(1+\tau s)} \tag{31}$$

If we put: $\frac{k_p}{k_i} = \tau$ then $H_{ol}(s) = \frac{kk_i}{s}$

The closed loop transfer function of the global system is given by:

$$H_{cl}(s) = \frac{1}{1+\frac{1}{kk_i}s} \tag{32}$$

The time response for a feedback system to get a 95% of the reference is given by: $t_r = 3\frac{1}{kk_i}$

Because: $\frac{k_p}{\tau} = k_i$ then $t_r = 3\frac{\tau}{kk_p}$

From which it can be deduced that: $k_p = 3\frac{\tau}{kt_r}$ and $k_i = 3\frac{1}{kt_r}$

ACKNOWLEDGMENT

The authors extend their appreciation to the Deanship of Scientific Research at King Khalid University under for funding this work through General Research Project under Grant number (RGP.1/373/44).

REFERENCES

[1] P. Naganathan and S. Srinivas, "Direct torque control techniques of three-level H-bridge inverter fed induction motor for torque ripple reduction at low speed operations," *IEEE Trans. Ind. Electron.*, vol. 67, no. 10, pp. 8262–8270, Oct. 2020, doi: 10.1109/tie.2019.2950840.

[2] A. Fereidooni, S. A. Davari, C. Garcia, and J. Rodriguez, "Simplified predictive stator current phase angle control of induction motor with a reference manipulation technique," *IEEE Access*, vol. 9, pp. 54173–54183, 2021, doi: 10.1109/access.2021.3070790.

[3] S. Savarapu, Md. Qutubuddin, and Y. Narri, "Modified brain emotional controller-based ripple minimization for SVM-DTC of sensorless induction motor drive," *IEEE Access*, vol. 10, pp. 40872–40887, 2022, doi: 10.1109/access.2022.3165651.

[4] I. Sami, S. Ullah, A. Basit, N. Ullah, and J. Ro, "Integral super twisting sliding mode based sensorless predictive torque control of induction motor," *IEEE Access*, vol. 8, pp. 186740–186755, 2020, doi: 10.1109/access.2020.3028845.

[5] X. Wu, W. Huang, X. Lin, W. Jiang, Y. Zhao, and S. Zhu, "Direct torque control for induction motors based on minimum voltage vector error," *IEEE Trans. Ind. Electron.*, vol. 68, no. 5, pp. 3794–3804, May 2021, doi: 10.1109/tie.2020.2987283.

[6] M. H. Holakooie and G. Iwanski, "Virtual subspace-based DTC strategy for torque ripple minimization in six-phase induction motors," *IEEE Access*, vol. 9, pp. 154692–154703, 2021, doi: 10.1109/ACCESS.2021.3128759.

[7] M. Nagataki, K. Kondo, O. Yamazaki, K. Yuki, and Y. Nakazawa, "Online auto-tuning method in field-orientation-controlled induction motor driving inertial load," *IEEE Open J. Ind. Appl.*, vol. 3, pp. 125–140, 2022, doi: 10.1109/ojia.2022.3189343.

[8] L. Cheng and M. Tsai, "Enhanced model predictive direct torque control applied to IPM motor with online parameter adaptation," *IEEE Access*, vol. 8, pp. 42185–42199, 2020, doi: 10.1109/access.2020.2977057.

[9] I. M. Alsofyani, Y. Bak, and K. Lee, "Fast torque control and minimized sector-flux droop for constant frequency torque controller based DTC of induction machines," *IEEE Trans. Power Electron.*, vol. 34, no. 12, pp. 12141–12153, Dec. 2019, doi: 10.1109/tpel.2019.2908631.

[10] J. Rodriguez, P. Cortes, R. Kennel, and M. Kazmierkowski, "Model predictive control—A simple and powerful method to control power converters," in *Proc. IEEE 6th Int. Power Electron. Motion Control Conf.*, May 2009, pp. 1–6, doi: 10.1109/IPEMC.2009.5289335.

[11] K. Belda and D.Vošmik, "Explicit generalized predictive algorithms for speed control of PMSM drives," in *Proc. 39th Annu. Conf. IEEE Ind. Electron. Soc.*, Nov. 2013, pp. 2833–2838, doi: 10.1109/IECON.2013.6699580.

[12] E. S. de Santana, E. Bim, and W. C. do Amaral, "A predictive algorithm for controlling speed and rotor flux of induction motor," *IEEE Trans. Ind. Electron.*, vol. 55, no. 12, pp. 4398–4407, Dec. 2008, doi: 10.1109/TIE.2008.2007376.

[13] H. Mesloub, M. T. Benchouia, A. Goléa, N. Goléa, and M. E. H. Benbouzid, "Predictive DTC schemes with PI regulator and particle swarm optimization for PMSM drive: Comparative simulation and experimental study," *Int. J. Adv. Manuf. Technol.*, vol. 86, nos. 9–12, pp. 3123–3134, Oct. 2016, doi: 10.1007/s00170-016-8406-x.

[14] M. Salehifar and M. Moreno-Equilaz, "Fault diagnosis and fault-tolerant finite control set-model predictive control of a multiphase voltage-source inverter supplying BLDC motor," *ISA Trans.*, vol. 60, pp. 143–155, Jan. 2016, doi: 10.1016/j.isatra.2015.10.007.

[15] W. Xie, X. Wang, F. Wang, W. Xu, R. M. Kennel, D. Gerling, and R. D. Lorenz, "Finite-control-set model predictive torque control with a deadbeat solution for PMSM drives," *IEEE Trans. Ind. Electron.*, vol. 62, no. 9, pp. 5402–5410, Sep. 2015, doi: 10.1109/TIE.2015.2410767.

[16] Y. Zhang and H. Yang, "Generalized two-vector-based model-predictive torque control of induction motor drives," *IEEE Trans. Power Electron.*, vol. 30, no. 7, pp. 3818–3829, Jul. 2015, doi: 10.1109/TPEL.2014.2349508.

[17] V. P. Muddineni, A. K. Bonala, and S. R. Sandepudi, "Enhanced weighting factor selection for predictive torque control of induction motor drive based on VIKOR method," *IET Electr. Power Appl.*, vol. 10, no. 9, pp. 877–888, Nov. 2016, doi: 10.1049/iet-epa.2016.0057.

[18] F. Wang, Z. Zhang, A. Davari, J. Rodríguez, and R. Kennel, "An experimental assessment of finite-state predictive torque control for electrical drives by considering different online-optimization methods," *Control Eng. Pract.*, vol. 31, pp. 1–8, Oct. 2014, doi: 10.1016/j.conengprac.2014.06.004.

[19] I. Maaoui-Ben Hassine, M. W. Naouar, and N. Mrabet-Bellaaj, "Predictive control strategies for wind turbine system based on permanent magnet synchronous generator," *ISA Trans.*, vol. 62, pp. 73–80, May 2016, doi: 10.1016/j.isatra.2015.12.002.

[20] M. Habibullah, D. D.-C. Lu, D. Xiao, and M. F. Rahman, "A computationally efficient FS-PTC for IM with minimum voltage vectors," in *Proc. IEEE 11th Int. Conf. Power Electron. Drive Syst.*, Jun. 2015, pp. 992–997.

[21] O. Naifar, G. Boukettaya, and A. Ouali, "Global stabilization of an adaptive observer-based controller design applied to induction machine," *Int. J. Adv. Manuf. Technol.*, vol. 81, nos. 1–4, pp. 423–432, Oct. 2015, doi: 10.1007/s00170-015-7099-x.

[22] M. H. Holakooie, M. Ojaghi, and A. Taheri, "Full-order Luenberger observer based on fuzzy-logic control for sensorless field-oriented control of a single-sided linear induction motor," *ISA Trans.*, vol. 60, pp. 96–108, Jan. 2016, doi: 10.1016/j.isatra.2015.11.022.

[23] F. Wang, Z. Zhang, R. Kennel, and J. Rodríguez, "Model predictive torque control with an extended prediction horizon for electrical drive systems," *Int. J. Control*, vol. 88, no. 7, pp. 1379–1388, Jul. 2015, doi: 10.1080/00207179.2014.942698.

[24] K. Szabat, P. Serkies, and T. Orłowska-Kowalska, "Application of the long-horizon predictive control to the drive system with elastic joint," in *Advanced and Intelligent Control in Power Electronics and Drives*, 2014, pp. 249–265.

[25] C. Xia, T. Liu, T. Shi, and Z. Song, "A simplified finite-control-set model-predictive control for power converters," *IEEE Trans. Ind. Informat.*, vol. 10, no. 2, pp. 991–1002, May 2014, doi: 10.1109/TII.2013.2284558.

[26] M. Habibullah, D. D. Lu, D. Xiao, and M. F. Rahman, "A simplified finite-state predictive direct torque control for induction motor drive," *IEEE Trans. Ind. Electron.*, vol. 63, no. 6, pp. 3964–3975, Jun. 2016, doi: 10.1109/TIE.2016.2519327.

[27] F. Wang, S. Li, X. Mei, W. Xie, J. Rodríguez, and R. M. Kennel, "Model-based predictive direct control strategies for electrical drives: An experimental evaluation of PTC and PCC methods," *IEEE Trans. Ind. Informat.*, vol. 11, no. 3, pp. 671–681, Jun. 2015, doi: 10.1109/TII.2015.2423154.

[28] J. Rodriguez, R. M. Kennel, J. R. Espinoza, M. Trincado, C. A. Silva, and C. A. Rojas, "High-performance control strategies for electrical drives: An experimental assessment," *IEEE Trans. Ind. Electron.*, vol. 59, no. 2, pp. 812–820, Feb. 2012, doi: 10.1109/TIE.2011.2158778.

[29] Md. Habibullah, D. D. Lu, D. Xiao, and M. F. Rahman, "Finite-state predictive torque control of induction motor supplied from a three-level NPC voltage source inverter," *IEEE Trans. Power Electron.*, vol. 32, no. 1, pp. 479–489, Jan. 2017, doi: 10.1109/TPEL.2016.2522977.

[30] P. Cortes, J. Rodriguez, C. Silva, and A. Flores, "Delay compensation in model predictive current control of a three-phase inverter," *IEEE Trans. Ind. Electron.*, vol. 59, no. 2, pp. 1323–1325, Feb. 2012, doi: 10.1109/TIE.2011.2157284.

MOHAMED CHEBAANI was born in Biskra, Algeria. He received the master's and Ph.D. degrees in electrical engineering from the University of Biskra, Algeria, in 2014 and 2020, respectively. He is currently a Teaching Assistant with the Department of Electrical Engineering, University of Biskra. His research interests include electric machines and drives, power electronics, and renewable energy applications.

MOHAMED EBEED received the B.S. degree from Aswan University, Egypt, in 2005, the M.S. degree in electrical engineering from South Valley University, in 2013, and the jointly-supervised Ph.D. degree from the Department of Electrical Engineering, Faculty of Engineering, Aswan University, and the University of Jaén, Spain, in 2018. From 2008 to 2009, he was a Lecturer with the Aswan Technical Institute. From 2009 to 2017, he was a Maintenance Engineer with EFACO Company. He is currently an Assistant Professor with the Department of Electrical Engineering, Faculty of Engineering, Sohag University, Egypt.

WALID S. E. ABDELLATIF was born in Kafr El-Sheikh, Egypt. He received the B.Sc. degree in industrial education and the master's degree in industrial education (electrical power and machines) from Suez Canal University, Suez, Egypt, in 2006 and 2012, respectively, and the Ph.D. degree from the Electrical Department, Faculty of Industrial Education, Suez University, Suez, in 2016. Since 2016, he has been an Assistant Professor with the Electricity Department (Electrical Power and Machines), Faculty of Technology and Education, Suez University. His research interests include renewable energy sources especially wind energy issues, power electronics, micro grid, and power quality.

Z. M. SALEM ELBARBARY was born in Kafr El-Sheikh, Egypt, in April 1971. He received the B.Sc., M.Sc., and Ph.D. degrees in electrical engineering from Menoufia University, Egypt, in 1994, 2002, and 2007, respectively. In 2009, he joined Kafrelshikh University, as an Assistant Professor. In 2016, he was a Research Visitor with Ghent University, Ghent, Belgium, for two months. In June 2022, he was promoted to a Full Professor in power electronics. His research interests include the control of electrical machines, senseless control, the applications of power electronics, real-time control using digital signals processing, and renewable energy applications.

NOURA A. NOURALDIN received the B.S. degree from Suez University, Suez, Egypt, in 2011, and the M.S. and Ph.D. degrees from the Electrical Department (Electrical Power & Machines), Suez University, in 2016 and 2022, respectively. Since 2012, she has been a Lecturer with the Electrical Department (Electrical Power & Machines), Suez University. Her research interests include renewable energy sources, especially the wind turbines and PV energy issues, power electronics, micro grid, and power quality.